EurJIC European Journal of Inorganic Chemistry
ChemPubSoc Europe
FULL PAPER

DOI:10.1002/ejic.201402473

Nanomolar Detection of Ag^I Ions in Aqueous Medium by Using Naphthalimide-Based Imine-Linked Fluorescent Organic Nanoparticles – Application in Environmental Samples

Hemant Sharma,[a] Vimal K. Bhardwaj,[a] and Narinder Singh*[a]

Keywords: Analytical methods / Sensors / Fluorescence / Nanomolar detection / Silver / Environmental chemistry

The synthesis of fluorescent organic nanoparticles (FONPs) with an imine-linked 1,8-naphthalimide-based dipodal chemosensor for Ag^I is described. The FONPs were prepared by using a re-precipitation method, and they were successfully applied for the nanomolar detection of Ag^I ions in aqueous media. More specifically, the chemosensor was utilized for the selective and ratiometric sensing of Ag^I in a concentration range 15–65 nM with a 15.5 nM detection limit. The work was extended to monitor the Ag^I concentration in samples of environmental importance.

Introduction

Over the past 20 years, a wide range of industrial uses for silver have been, and continue to be, introduced.[1] From organic catalysis to non-corroding electrical switches, silver is extensively used in every industry.[2–4] The main applications are coins and medals, jewelry, electronics, and in the imaging industry.[5,6] The large-scale use of silver leads to its slow discharge into the environment.[7,8] The alarming impact of silver ions, especially, on flora and fauna has received much attention.[8] Silver can inactivate sulfhydryl enzymes and accumulate in the body, where it causes the irreversible darkening of the skin and mucous membranes.[9,10] A number of analytical methods are available in the literature for the estimation of silver ion concentration; however, they suffer from being costly, time-consuming, and tedious protocols.[11,12] The development of fluorescent chemosensors with high sensitivity, high selectivity, a low detection limit, and a broad detection range has been receiving considerable attention because of their vital role in biological, medical, and environmental analysis.[13] However, the detection of silver in aqueous medium remains challenging because of the low solubility of chemosensors in aqueous medium. Silver does not have an intrinsic spectroscopic or magnetic signal (silent ion), and it is therefore very difficult to differentiate from other chemically closely related ions. In this regard, considerable efforts have been made to synthesize Ag^I-selective fluorescent chemosensors that can detect Ag^I in organic solvents and aqueous solutions selectively;[13–18] contrary to this, only few reports are available about ratiometric fluorescent sensors for the Ag^I ion.[19]

To the best of our knowledge, there are no reports about fluorescent organic nanoparticles (FONPs) used for the ratiometric estimation of Ag^I in aqueous medium, although many other metal ions have been investigated. Here, FONPs were prepared by using naphthalimide-based imine-linked dipodal chemosensors for the nanomolar detection of Ag^I in water. Organic nanoparticles (ONPs) offer many advantages, like their solubility in aqueous systems, which helps to avoid toxic organic solvents, real-time detection, a broad detection range, and a low detection limit.[16,20–27] There are several methods to prepare ONPs, such as emulsion, drying, and re-precipitation. The re-precipitation method has been employed for the synthesis of imine-linked dipodal ONPs. The role of imine linkages for the binding of Ag^I in receptor pseudocavity has already been established.[28] In the design of the present investigation, the sp^2 nitrogen binding sites from imine linkages are provided in such a way that the receptor should offer five-membered chelate ring.

Results and Discussion

Synthesis of the Chemosensors

Chemosensor **1** was synthesized through a series of steps, as illustrated in Scheme 1. The compounds **2** and **4** were synthesized by using literature methods.[29,30] The dipodal aldehydes **3a** and **3b** were synthesized by the nucleophilic reaction of dibromide **2** with 2-hydroxybenzaldehyde and 3-hydroxybenzaldehyde, respectively, under basic conditions.

[a] Department of Chemistry, Indian Institute of Technology Ropar (IIT Ropar),
Rupnagar, Panjab 140001, India
E-mail: nsingh@iitrpr.ac.in
http://www.iitrpr.ac.in/chemistry/nsingh

Supporting information for this article is available on the WWW under http://dx.doi.org/10.1002/ejic.201402473.

A purification by column chromatography on silica gel yielded the pure products **3a** and **3b** in 78 and 75% yield, respectively.

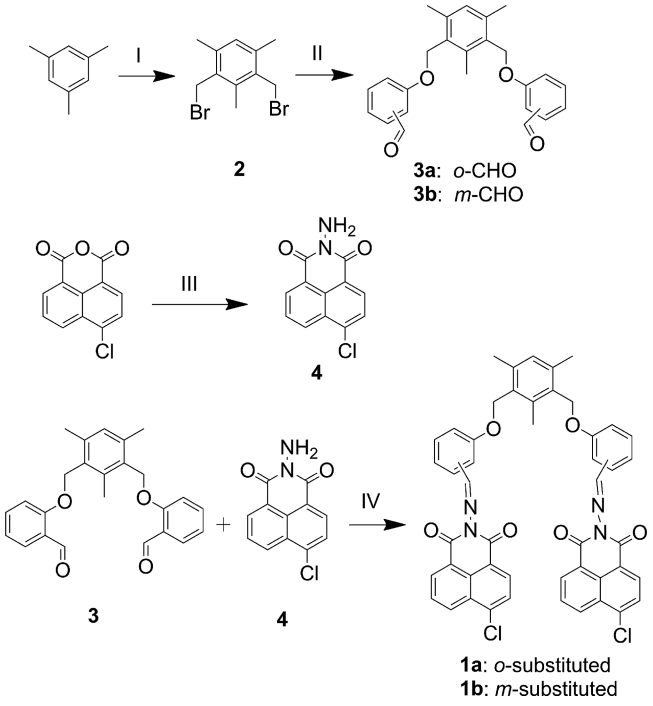

Scheme 1. Synthesis of imine-linked 1,8-naphthalimide-based dipodal chemosensors. Reagents and conditions: (I) $(HCHO)_n$, HBr in acetic acid, reflux for 15 h; (II) K_2CO_3, CH_3CN, $TBAHSO_4$, 2-hydroxy benzaldehyde or 3-hydroxy benzaldehyde, reflux for 15 h; (III) NH_2–NH_2, ethanol, stir for 5 h; (IV) $CHCl_3/CH_3OH$ (1:1), reflux for 12 h.

A condensation reaction between dialdehydes **3a** and **3b** and amine **4** yielded the imine-linked chemosensors **1a** and **1b**, respectively, in 64 and 66% yield, respectively. These new compounds were fully characterized with spectroscopic methods, which includes ^{1}H NMR spectroscopy, where a singlet signal at 8.65 and 8.74 ppm is observed for **1a** and **1b**, respectively, which is assigned to the imine linkages (–CH=N), as shown in Figures S1–S4. To support the proposed sensor activity for ions, compounds **5** and **6** were synthesized in 67 and 66% yield, respectively, by using a literature method (Scheme 2).[22,30,31]

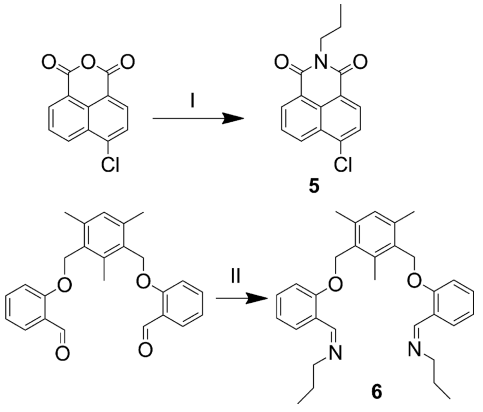

Scheme 2. Synthesis of controls **5** and **6**. Reagents and conditions: (I) *n*-propylamine, reflux overnight; (II) *n*-propylamine, CH_3CN, reflux for 12 h.

Preparation of ONPs and Recognition Studies

The re-precipitation method was employed for the preparation of ONPs. The receptor **1** (2 mg) was dissolved in 10 mL of THF, and the solution was filtered through a porous membrane (pore size of 0.3 μm). This solution was rapidly injected into 990 mL of highly purified water with sonication for 15 min at room temperature. The solution was kept for 5 h to check the stability of the system. The UV/Vis spectra of receptors **1a** and **1b** were recorded in pure THF, and they exhibit a broad band in the visible region (453 nm and 443 nm, respectively), as shown in Figure 1 (A). In aqueous media, a significant bathochromic shift was observed in both cases. The receptors **1a** and **1b** have absorbance maxima at 460 nm and 453 nm, respectively, in aqueous media (Figure 1, A). Further, emission spectra of **1a** and **1b** were recorded in pure THF and water (Figure 1, B). In the case of **1a**, an enhancement in the emission intensity and a slight redshift were observed (Figure 1, B). A similar response was seen for **1b**, however, with more a prominent enhancement and a redshift in the peak (Figure 1, B). This dramatic change in the photophysical properties of **1a** and **1b** can be explained on the basis of the formation of organic nanoparticles (ONPs). On formation of ONPs, the rigidity increases in the molecule, which leads to a prevention of non-radiative decay and enhances the fluorescence intensity with a redshift.[32] To explore the effect of water content on the formation of ONPs, emission spectra of **1a** and **1b** were recorded in different media with a varying water fraction between 0 and 99% (Figure 1, C

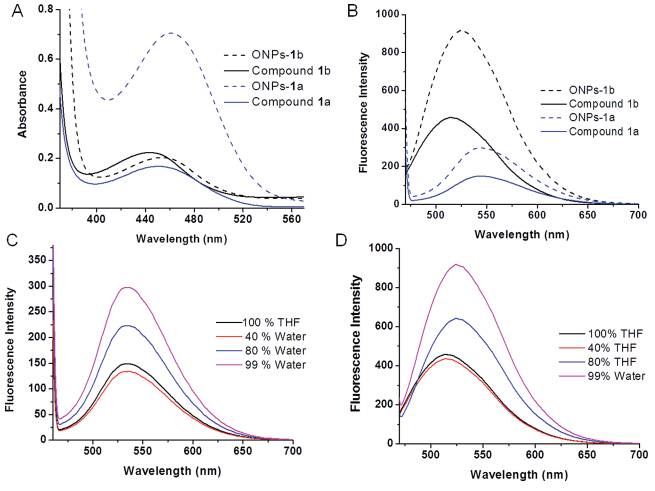

Figure 1. (A) Absorbance spectra of compounds **1a** (10 μM) and **1b** (10 μM) in THF and of ONPs of **1a** (2.3 μM) and **1b** (2.3 μM) in water. (B) Emission spectra of compounds **1a** (10 μM) and **1b** (10 μM) in THF and of ONPs of **1a** (2.3 μM) and **1b** (2.3 μM) in water. (C) Change in the emission profile of **1a** upon varying the water fraction. (D) Change in emission profile of **1b** upon varying the water fraction.

and D). During the course of ONP development, the size and distribution of ONPs were determined with the external-probe feature of dynamic light scattering (DLS). The external-probe feature of DLS allows to continuously and rapidly monitor the size of ONPs. The external probe equipped with a laser diode was dipped in the solutions. It is worth noting that in media 80% or more water the formation of ONPs could be achieved, as shown in Figure S5.

Beyond 80% water content, emission intensity as well as uniformity in the distribution of size were increased (see Figure 1, C and D and Supporting Information, Figure S5). Suitably uniform and nano-sized ONPs of **1a** and **1b** were obtained at 99% water content (Figures S5D and S5E). Moreover, the concentration for the formation of ONPs was optimized. The absorption and emission spectra of ONPs **1a** and **1b** were recorded at different concentrations, for example, 1.0, 2.3, 4.5, 7.0, and 10.0 μM (Figure 2). The concentration of receptor and the size of ONPs have a linear relationship. The size of ONPs increased with the concentration of **1a** and **1b** (Figure 2, E). The large ONPs have broad and prominent absorption bands (Figure 2, A and B). However, the emission intensity of ONPs increased with the concentration of receptor only up to a certain limit (Figure 2, C and D). Beyond 7.0 μM, quenching was observed. The possible reason behind the quenching is "aggregation-caused quenching" (ACQ).[33,34] The aromatic rings of naphthalimide undergo π–π stacking, which results in the formation of excimers. The excimers contribute towards the ACQ effect. Therefore, an optimized concentration (2.3 μM) was used in further studies. It gives appropriate absorption and emission profiles along with uniformly distributed ONPs in the range 98–102 nm (Figure 2, Figures S5D and S5E). The shape and size of ONPs of **1a** and **1b** were also characterized through TEM images, as shown in Figure 2 (F and G). The TEM analysis showed that discrete ONPs of **1a** and **1b** have a size of 20 and 25 nm, respectively (Figure 2, F and G). The difference in the sizes determined by TEM and DLS measurements is due to the fact that DLS measures the hydrodynamic size of nanoparticles, whereas TEM records the size of discrete particles. Moreover, the time of sonication also controls the size and quality of ONPs. A sonication less than 10 min produced large and unstable ONPs, which start to agglomerate with time.

The interaction of different metal ions with ONPs of **1a** and **1b** was examined. It was observed that none of the metal ions disturbed the absorbance profiles of **1a** and **1b** (Figures S6A and B). These results indicate a non-selective behavior of ONP of **1a** and **1b** in absorption spectroscopy. Further, the emission profiles of ONP**1a** and ONP-**1b** were recorded with various metal ions. The emission profile of ONP-**1b** showed a significant change with Ag^I ions, as shown in Figure 3 (A). The addition of Ag^I ions produced a ratiometric change in the emission profile of ONP-**1b**. Two

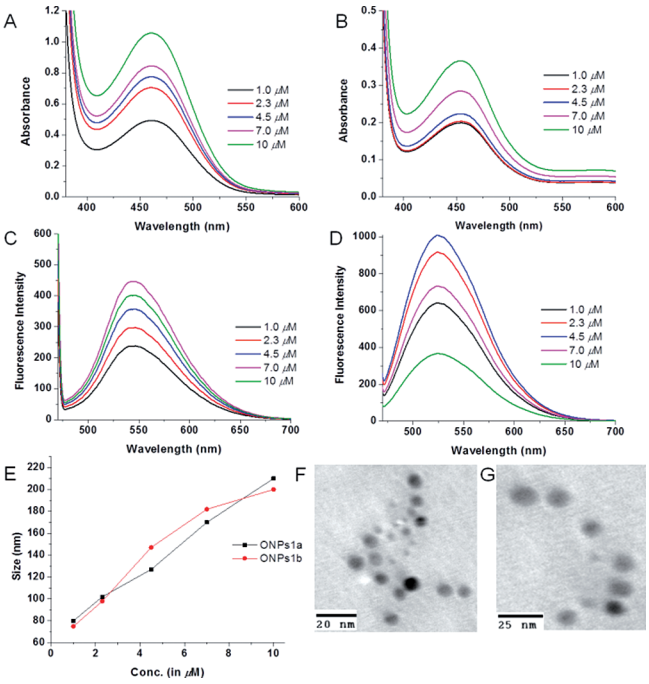

Figure 2. (A) Effect on the absorption spectra of ONPs of **1a** upon changing the concentration of **1a**. (B) Effect on the absorption spectra of ONPs of **1b** upon changing the concentration of **1b**. (C) Effect on the emission spectra of ONPs of **1a** upon changing the concentration of **1a**. (D) Effect on the emission spectra of ONPs of **1b** upon changing the concentration of **1**b. (E) Variation in size of ONPs of **1a** and **1b** as a function of the concentration of compounds **1a** and **1b** in water. (F) TEM images of ONPs of **1a** (20 nm) and (G) TEM images of ONPs of **1b** (25 nm).

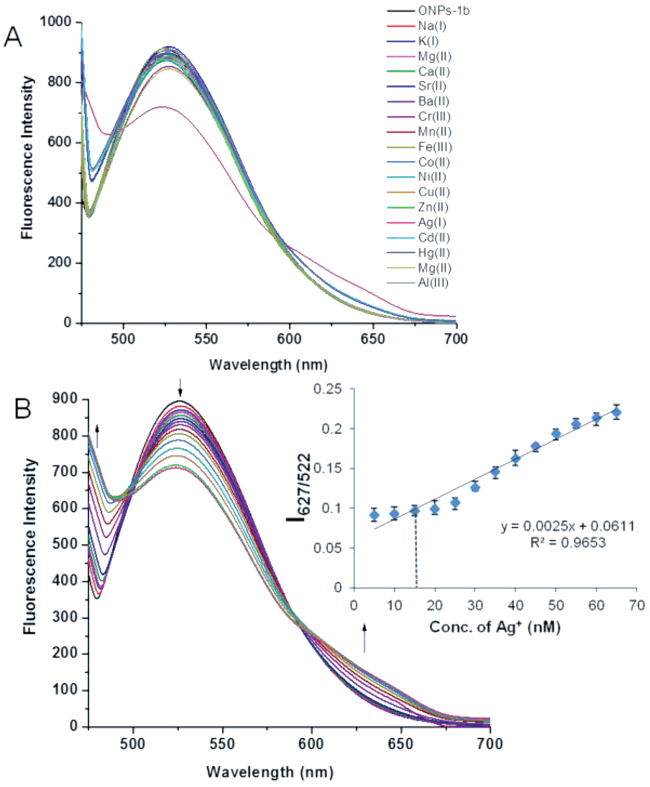

Figure 3. (A) Changes in the fluorescence spectra of ONP-**1b** (2.3 μM) in the presence of different metal nitrate salts (100 nM) in aqueous media. (B) Changes in the fluorescence spectra of ONP-**1b** (0.2 μM) upon successive addition of Ag^I ions (0–70 nM); inset shows the linear relationship between ratiometric intensity ($I_{627/522}$) and concentration of Ag^I ion.

isosbestic points were observed at 496 and 587 nm (Figure 3, A). To study this in more detail, a of ONP-**1b** was titrated with small aliquots of Ag^I ions. Upon addition of Ag^I ions, the emission intensity of ONP-**1b** was quenched at 522 nm and enhanced at 627 nm, which is consistent with the clear isoemissive points shown in Figure 3 (B). To find the linear range of detection, the ratiometric fluorescence intensity ($I_{627}/_{522}$) was plotted against the concentration of Ag^I ions. A linear relationship was observed in the concentration range 15–65 nM (inset of Figure 3, B). The minimum detection limit was calculated to be 15.5 nM. It was hypothesized that the shape and size of the ONPs is influenced after interacting with Ag^I ions. Therefore, SEM images of ONP-**1b** before and after treatment with Ag^I were recorded. ONPs of **1b** are spherical in shape, as shown in Figure S7A. However, a robust change in the morphology of ONPs-**1b** was seen after interacting with Ag^I ion, and big clumps were observed (Figures S7A and B). This means that the Ag^I ions interact on the surface of the ONPs and initialize the aggregation of particles. The increase in particle size was also confirmed by DLS studies. The size of the ONPs was increased with a broad distribution in size and a maximum at about 190 nm (Figure S7B).

The binding constant and stoichiometry were calculated by using the Lehrer–Chipman Equation (1) for a (Ag^+_n·**1**) complex.[35,36]

$$\ln[(F - F_0)/(F_\infty - F)] = n\ln[Ag^+] + n\ln(K_{asscn}) \quad (1)$$

The symbol n corresponds to the number of Ag^I ions attached to each molecule of **1b**, K_{asscn} is the binding constant, F_0 is the fluorescence intensity of receptor **1b** only, F is the fluorescence intensity of **1b** at a particular concentration of Ag^I ions, and F_∞ is the fluorescence intensity of **1b** at maximum concentration. The slope of the plot of $\ln[(F - F_0)/(F_\infty - F)]$ against $\ln[Ag^+]$ gave the stoichiometry, and it is about 2.0, which corresponds to a 1:2 ratio between host and guest (Figure S8). The intercept of the plot gave the binding constant of **1b**·Ag^+, and it is about $4.5(\pm 0.4) \times 10^5$ M^{-2}. To further confirm the stoichiometry between ONP-**1b** and Ag^I ions, a Job plot was drawn between compound **1** and Ag^I in pure THF. The concentration of the host–guest complex [HG] was plotted against {[G]/([H] + [G])}, where [G] is the concentration of the guest Ag^I and [H] is the concentration of the host ONP-**1b**, and the plot has maximum at 0.7, which corresponds to a 1:2 stoichiometry between host and guest molecule (Figure S9). Furthermore, the effect of pH on the emission profile of ONP-**1b** was evaluated. To perform this experiment, emission spectra of ONP-**1b** were recorded in aqueous media with varying pH (by using HCl and tetrabutylammonium hydroxide). It is noteworthy that ONP-**1b** is quite resistant to show any change in the emission profile upon varying the pH of the solution (Figure 4, A and B).

This wide operational pH range (2.3–12.3) increased the scope of ONP-**1b** as a sensor for Ag^I ions. To evaluate the effect of pH on the recognition of Ag^I ions, a set of solutions of ONP-**1b** were prepared, which had different pH in the range 2–12. A solution of Ag^I ions (70 nM) was added

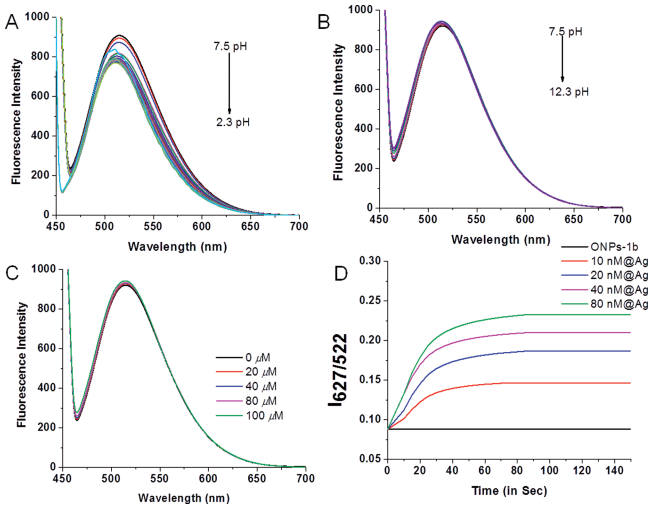

Figure 4. (A) Effect of acidic medium on the emission intensity of ONP-**1b** upon changing the pH of the solution (7.5–2.3). (B) Effect of basic medium on emission intensity of ONP-**1b** upon changing the pH of the solution from (7.5–12.3). (C) Changes in emission intensity of ONP-**1b** upon changing the ionic strength of the solution (0–100 μM, $TBAClO_4$). (D) Plot of fluorescence intensity of ONP-**1b** and Ag^I at different concentrations as a function of time (sec).

to the ONP-**1b** solutions, and fluorescence spectra were recorded, as shown in Figure S10A. The fluorescence intensity at 522 nm was plotted against the pH of the solution (Figure S10A). It was noticed that the change was almost similar in all cases, which means that the pH of the solution does not interfere with the recognition of Ag^I ions. Additionally, the effects of the ionic strength on the emission profile of ONP-**1b** were examined by using various concentrations (0–100 μM) of tetrabutylammonium perchlorate ($TBAClO_4$), as shown in Figure 4 (C). The results show that even 100 μM of $TBAClO_4$ do not affect the emission profile of the ONP-**1b**. Similar to pH studies, the detection of Ag^I was executed in solutions of varying ionic strength (0–100 μM). Figure S10B shows that the response of ONP-**1b** towards Ag^I ions remains same in solutions of different ionic strength. Moreover, response time is one of the key factors for real-time sensing of Ag^I ions. To calculate the response time of ONP-**1b** for Ag^I, a set of solutions were prepared with different concentrations of Ag^I ions, and the ratiometric fluorescence intensity ($I_{627/522}$) was measured as a function of time, as shown in Figure 4 (D). The response time of ONP-**1b** for Ag^I does not depend on the concentration of the Ag^I ions; in each case, 84 s is sufficient to reach the equilibrium. Figure 4 (D) illustrates that once the equilibrium was reached, no change in the ratiometric intensity at ($I_{627/522}$) was observed, which indicates the stability of the system. Moreover, selectivity is another deciding factor for good sensing; the emission intensity at 522 nm of ONP-**1b** was measured in the presence and absence of equimolar amounts of other competing cations. It was noticed that ONP-**1b** recognized Ag^I ions selectively even in the presence of other competing cations (Figure 5). To illustrate the mechanism and the role of the moieties for the binding of

Ag^I ions, different derivatives of naphthalimide and dipodal aldehyde were prepared. The metal binding test of *ortho*-substituted **1a** was performed. Likewise, ONPs of **1a** were prepared by the re-precipitation method. Figure S11 indicates that ONP-**1a** shows a ratiometric response with Ag^I ions; however, the response is less prominent compared to ONP-**1b**. However, it also has a similar response with Cd^{II}, Hg^{II}, Co^{II}, and other transition metal ions. These results point out the non-selective behavior of ONP-**1a** towards cations. Further, to check the role of naphthalimide in metal binding, compound **5** was synthesized and subsequently used for ONP preparation. The metal-binding test results depict that ONP-**5** has a non-selective profile in emission spectroscopy (Figure S12A). Similarly, compound **6** was synthesized to evaluate the role of the dipodal aldehyde. ONP-**6** also exhibits a non-selective response to metal ions (Figure S12B).

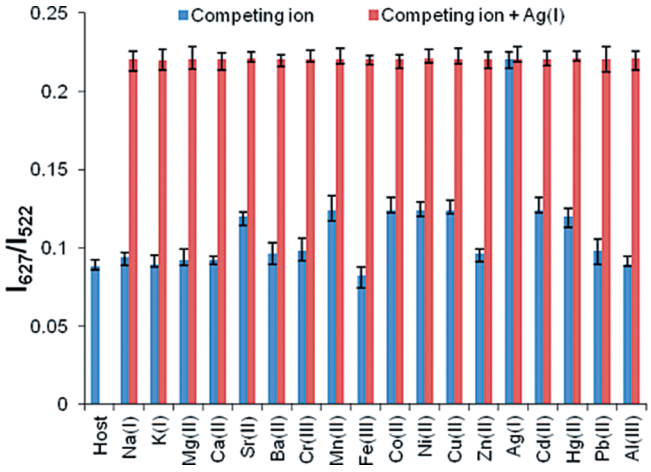

Figure 5. Estimation of Ag^I in the presence of other metal ions [Na^I, K^I, Mg^{II}, Ca^{II}, Sr^{II}, Ba^{II}, Cr^{III}, Mn^{II}, Fe^{III}, Co^{II}, Ni^{II}, Cu^{II}, Zn^{II}, Cd^{II}, Hg^{II}, Pb^{II}, and Al^{III}] in water.

These results inferred that the binding of Ag^I occurred only when the Schiff base was formed from **3** and **4**. Therefore, the binding site for Ag^I ions consists of the (–CH=N–) imine linkage along with the naphthalimide moiety, which provide the platform for this binding site, as shown in Scheme 3. The red hemisphere represents the binding site for Ag^I, and the other part provides the proper orientation of these binding sites (Scheme 3).

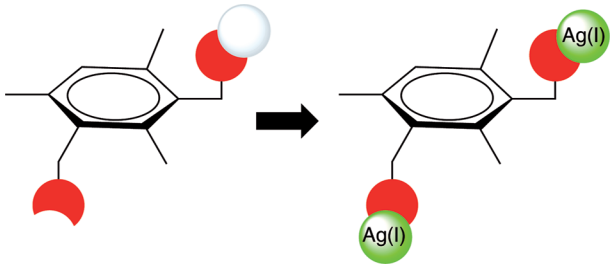

Scheme 3. Mechanism of Ag^I binding.

To understand the effect of Ag^I ions on the redox behavior of ONP-**1b**, cyclic voltammograms of ONP-**1b** were recorded in the presence and absence of Ag^I ions. The cyclic voltammogram of ONP-**1b** exhibits an oxidation wave at 0.040 V and a reduction wave at 0.486 V (Figure S13). The addition of a Ag^I solution (100 nM) led to a shift of the oxidation wave to higher potential; however, the reduction potential remained almost the same and showed an increase in the intensity of the wave, as shown in Figure S13. To check the nature of the binding interactions, tetrabutylammonium chloride (TBACl) was added to the above solution. After stirring for 5 min, the voltammogram was recorded. It was observed that ONP-**1b** regains its redox profile upon addition of TBACl, because the Cl^- anions extract the Ag^I ions from the binding sites (Figure S13). This means that the binding of Ag^I ions to ONP-**1b** occurs reversibly through non-covalent interactions. Interestingly, *ortho*-substituted ONP-**1a** also has a non-selective response. To explain this phenomenon, DFT calculations were carried out with a Becke three-parameterized Lee–Yang–Parr (B3LYP) exchange functional with a 6-31G and LANL2DZ basis sets for the receptors and their silver complexes, respectively.[37–41] On careful examination of the optimized geometries of **1a** and **1b**, we found that **1b** has a more symmetrical geometry, in which two pods are arranged in opposite direction (Figure 6, A and B). However, **1a** has a very compact shape, and most of the electronegative atoms are involved in H-bonding interactions.

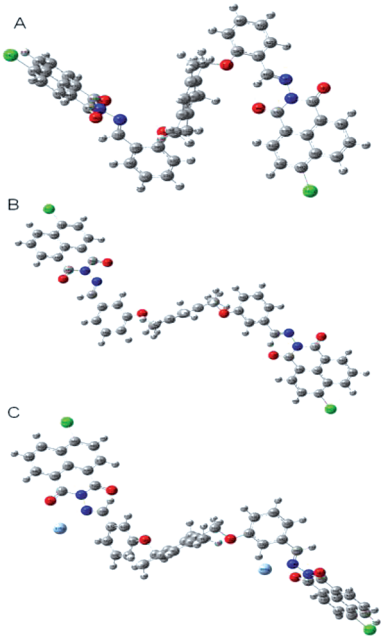

Figure 6. Energy-minimized optimized structures of the receptors **1a** and **1b**, and of the complex **1b**·Ag^I , calculated by using B3LYP/6-31G and B3LYP/LANL2DZ functional/basis set combinations, respectively. The red, blue, gray, dark green, and sea green spheres correspond to O, N, C, Cl, and Ag^I atoms, respectively.

Therefore, **1b** is more liable for binding as compared to **1a**, which is also confirmed by optimization energies, dipole moments, and $\Delta E_{HOMO-LUMO}$ (Table 1). These parameters

indicate the different configurations of **1a** and **1b**. Further, the Ag^I complex of **1b** was optimized by using the B3LYP functional with a LANL2DZ basis set (Figure 6, C).

Table 1. A comparison of optimized parameters of receptors **1a** and **1b** and of complex **1b**·Ag^I, calculated by using B3LYP/6-31G and B3LYP/LANL2DZ functional/basis set combinations, respectively.

	Energy [a.u.]	$\Delta E_{HOMO-LUMO}$ [a.u.]	Dipole moment [Debye]
1a	–3477.751	0.12742	4.689
1b	–3477.755	0.12737	5.188
1b·Ag^I	–2878.875	0.12109	10.783

The optimization parameters (energy and dipole moment) also point to a higher stability of **1b**·Ag^I (Table 1). To understand the molecular interactions upon binding, the orbital maps of the HOMOs and LUMOs of **1b** and **1b**·Ag^I were generated from the optimized geometries. The pictorial representations s show that HOMO and HOMO–1 are main contributors in the binding of Ag^I ions (Figure 7). Figure 7 also shows that the d_{z^2} orbital of the Ag^I is involved in the binding. The decrease of energy in the HOMO–LUMO gap also authenticate the binding phenomena.

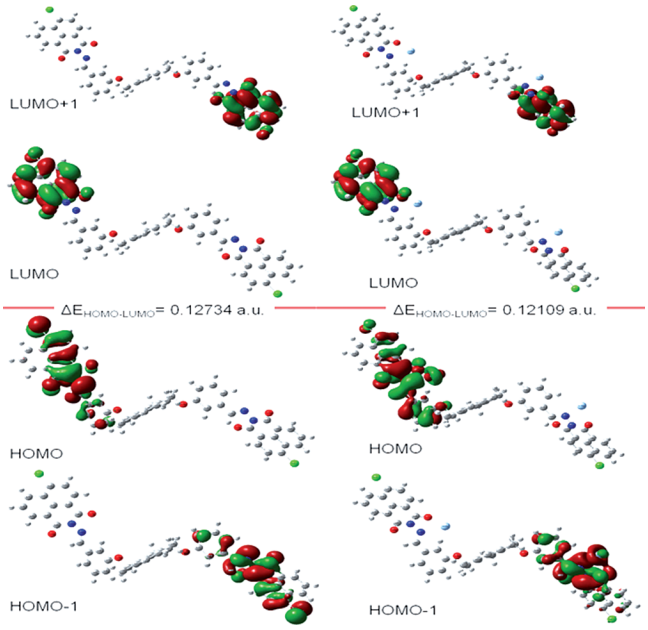

Figure 7. Representation of HOMO, HOMO–1, LUMO, and LUMO+1 of **1b** (left) and **1b**·Ag^I (right), calculated by using B3LYP/6-31G and B3LYP/LANL2DZ, respectively.

In jewelry industry, silver is extensively used for various purposes. With increasing demand of silver ornaments, the chance of contamination of natural resources like water is increasing. We randomly selected the effluent from Sarafa Bazaar in Ludhiana, India, one of the twenty most polluted cities in the world. The samples were centrifuged and filtered before analysis. The silver content of these samples was also monitored through inductively coupled plasma mass spectrometry (ICP-MS). The samples were collected on different days of the week, and results suggest that the content of silver varied from 17 to 35 nM (Table 2). These results are also in good agreement with the data obtained from ICP-MS, as shown in Table 2.

Table 2. Comparison of results obtained from Ag^I analyses with ONP-**1b** and ICP-MS.

Sample code	ONP-**1b** [nM](average)[a]	ICP-MS [nM] (average)[a]
E1	19 ± 0.2	20.2 ± 0.5
E2	21 ± 0.1	21.4 ± 0.4
E3	35 ± 0.4	34.9 ± 0.1
E4	20 ± 0.6	21.1 ± 0.2
E5	32 ± 0.3	32.3 ± 0.6
E6	17 ± 0.5	18.1 ± 0.2
E7	22 ± 0.2	22.4 ± 0.4

[a] Average of three different readings.

Conclusions

The *ortho* (**1a**) and *meta* (**1b**) derivatives of imine-linked naphthalimide-based dipodal FONPs were synthesized. The FONP (of **1a** and **1b**) were treated with various metal ions; only ONP-**1b** was found to be a selective sensor for Ag^I ions. The broad range of operational pH (2.3–12.3), low detection limit (15.5 nM), short response time (84 s), and broad range of detection (15–65 nM) make it a valuable sensor for Ag^I detection. Further, control samples **5** and **6** were also prepared and evaluated their metal-binding properties. The results show that the imine-linkage is responsible for the binding site for Ag^I ions. Furthermore, DFT calculations were performed to elucidate the mechanism of binding.

Experimental Section

General Information: All chemicals were purchased from Sigma–Aldrich and used without any further purification. The NMR studies were carried out with a Avance-II (Bruker) instrument and a JEOL 300 NMR spectrometer by using TMS as an internal standard and $CDCl_3$ as the solvent (400 and 300 MHz for ^1H NMR and 100 and 75 MHz for ^{13}C NMR). The UV/Vis absorption measurements were performed with a Specord 250 Plus Analytikjena spectrometer. A Perkin–Elmer L55 fluorescence spectrophotometer was employed for fluorescence measurements and equipped with a quartz cuvettes of 1 cm path length and a xenon lamp as the excitation source. TEM images were recorded with a Hitachi (H-7500) instrument operating at 80 kV. A 400-mesh carbon-coated copper grid was used for sample preparation. The size distribution of nanoparticles was determined with a Metrohm Microtrac Ultra Nanotrac particle-size analyzer (dynamic light scattering). The pH measurements were made with a Toshcon lab pH meter. The electrochemical measurements were recorded with a Potentiostat–Galvanostat BASI EPSILON instrument by using a Pt disk as the working electrode, an Ag/AgCl electrode as the reference (3 M KCl), and a Pt wire as the counter electrode. An Agilent 7700 Series ICP mass spectrometer was used for the determination of silver content

in water samples. The ICP-MS instrument was equipped with a ASX-500 series ICP-MS auto-sampler.

Compound 1a: Compound **4** was prepared according to a literature method.[30] The compounds **3a** (500 mg, 1 mmol) and **4** (635 mg, 2 mmol) were dissolved in $CHCl_3/CH_3OH$ (1:1) and heated at reflux for 12 h, yield 64%, m.p. ≥ 250 °C. ^{1}H NMR (300 MHz, $CDCl_3$): δ = 2.20 (s, 6 H, –CH_3), 2.29 (s, 3 H, –CH_3), 4.99 (s, 4 H, –CH_2), 6.71 (s, 1 H, –Ar), 6.98–7.03 (m, 4 H, –Ar), 7.40 (t, J = 7.2 Hz, 2 H, –Ar), 7.57–7.69 (m, 4 H, –Ar), 8.20 (d, J = 7.8 Hz, 4 H, –Ar), 8.35–8.40 (m, 4 H, –Ar), 8.65 (s, 2 H, –CH=N) ppm. ^{13}C NMR (75 MHz, $CDCl_3$): δ = 15.59, 19.96, 66.15, 96.31, 113.04, 121.62, 122.0, 122.23, 123.50, 127.31, 127.77, 128.37, 128.46, 129.19, 130.33, 130.76, 131.18, 132.12, 133.75, 138.63, 138.76, 139.18, 159.21, 159.71, 159.95, 166.43 ppm. $C_{49}H_{34}Cl_2N_4O_6$ (845.74): calcd. C 69.59, H 4.05, N 6.62; found C 69.52, H 4.12, N 6.68.

Compound 1b: Compounds **3b** (500 mg, 1 mmol) and **4** (635 mg, 2 mmol) were dissolved in $CHCl_3/CH_3OH$ (1:1) and heated at reflux for 12 h, yield 66%, m.p. ≥ 250 °C. ^{1}H NMR (400 MHz, $CDCl_3$): δ = 2.17 (s, 3 H, –CH_3), 2.41 (s, 6 H, –CH_3), 5.16 (s, 4 H, –CH_2), 7.03 (s, 1 H, –Ar), 7.44–7.55 (m, 6 H, –Ar), 7.80–7.88 (m, 4 H, –Ar), 8.59–8.73 (m, 10 H, –Ar, –CH=N) ppm. ^{13}C NMR (100 MHz, $CDCl_3$): δ = 17.0, 20.66, 67.84, 114.12, 118.55, 122.66, 123.23, 125.32, 125.69, 127.41, 128.27, 128.65, 129.31, 129.77, 130.02, 130.13, 131.41, 134.21, 134.38, 134.76, 135.65, 138.06, 159.27, 160.74, 162.0 ppm. $C_{49}H_{34}Cl_2N_4O_6$ (845.74): calcd. C 69.59, H 4.05, N 6.62; found C 69.62, H 4.03, N 6.65.

Metal Ion Recognition Studies of 1a, 1b, 5 and 6: All recognition studies were performed at room temperature and in aqueous medium. FONPs were prepared by using a re-precipitation method. The respective compound (2 mg) was dissolved in THF and injected readily into highly purified water by using a micro-syringe under sonication. The sonication was continued for 15 min. Afterwards, the solution was kept for 5 h. A library of 18 different metal ions [Na^I, K^I, Mg^{II}, Ca^{II}, Sr^{II}, Ba^{II}, Cr^{III}, Mn^{II}, Fe^{III}, Co^{II}, Ni^{II}, Cu^{II}, Zn^{II}, Cd^{II}, Hg^{II}, Ag^I, Pb^{II}, and Al^{III}] was used for binding studies. The metal-binding studies were executed in 5 mL volumetric flasks. Each flask contained ONPs (2.3 μM) along with a particular metal nitrate (100 nM). The selected metal was titrated with ONPs in a stepwise manner by using 10 mL volumetric flasks. The pH titrations were performed by using dilute HCl and tetrabutylammonium hydroxide in 25 mL volumetric flasks. The salt effect was studied by using different concentrations of tetrabutylammonium perchlorate (0–100 μM). The response time was calculated through measuring the fluorescence intensity at two different wavelengths (522 and 627 nm), and the ratiometric fluorescence intensity ($I_{627/522}$) was plotted as a function of time (sec). The method of continuous variation (Job plot) was used to determine the stoichiometry of the complex formed between **1** and Ag^I. Ten 5 mL volumetric flasks were taken and each had a fixed total concentration but mol variation of **1** and Ag^I. The Job plot was drawn between [HG] and [G]/([H] + [G]), and the maxima in plot give a stoichiometry of the complex. The authenticity of the receptor was tested through interference studies. For interference studies, a number of solutions were made, which contained a stock solution of ONP-**1b** (2.3 μM) along with a fixed concentration of Ag^I both with and without other interfering metal salts in aqueous system.

Supporting Information (see footnote on the first page of this article): ^{1}H and ^{13}C NMR spectra of **1**a and **1b**; DLS analysis of **1a** and **1b**; absorbance profiles of **1a** and **1b** with various metals; SEM images, Job's plot, pH study and CV profile of **1b** with Ag^I ions.

Acknowledgment

V. K. B. is thankful to the Department of Science and Technology (DST) for the DST-INSPIRE Faculty fellowship and research grant (IFA-11CH-09).

[1] The Silver Institute, Washington, **2013**, https://www.silverinstitute.org/site/supply-demand/silver-demand/.
[2] L. Bau, P. Tecilla, F. Mancin, *Nanoscale* **2011**, *3*, 121.
[3] S. Cui, H. Pu, E. C. Mattson, G. Lu, S. Mao, M. Weinert, C. J. Hirschmugl, M. Gajdardziska-Josifovska, J. Chen, *Nanoscale* **2012**, *4*, 5887.
[4] S. Yao, Y. Zhu, *Nanoscale* **2014**, *6*, 2345.
[5] H. T. Ratte, *Environ. Toxicol. Chem.* **1999**, *18*, 89.
[6] J. L. Barriada, A. D. Tappin, E. H. Evans, E. P. Achterberg, *Trac. Trends Anal. Chem.* **2007**, *26*, 809.
[7] B. Valeur, I. Leray, *Coord. Chem. Rev.* **2000**, *205*, 3.
[8] L. Prodi, F. Bolletta, M. Montalti, N. Zaccheroni, *Coord. Chem. Rev.* **2000**, *205*, 59.
[9] Q. L. Feng, J. Wu, G. Q. Chen, F. Z. Cui, T. N. Kim, J. O. Kim, *J. Biomed. Mater. Res.* **2000**, *52*, 662.
[10] X.-B. Zhang, Z.-X. Han, Z.-H. Fang, G.-L. Shen, R.-Q. Yu, *Analytica. Chim. Acta* **2006**, *562*, 210.
[11] D. Karunasagar, J. Arunachalam, S. Gangadharan, *J. Anal. At. Spectrom.* **1998**, *13*, 679.
[12] Y. Li, C. Chen, B. Li, J. Sun, J. Wang, Y. Gao, Y. Zhao, Z. Chai, *J. Anal. At. Spectrom.* **2006**, *21*, 94.
[13] J. F. Zhang, Y. Zhou, J. Yoon, J. S. Kim, *Chem. Soc. Rev.* **2011**, *40*, 3416.
[14] J. Hatai, S. Pal, S. Bandyopadhyay, *RSC Adv.* **2012**, *2*, 10941.
[15] K. M. K. Swamy, H. N. Kim, J. H. Soh, Y. Kim, S.-J. Kim, J. Yoon, *Chem. Commun.* **2009**, 1234.
[16] Y. Yue, T.-Y. Liu, H.-W. Li, Z. Liu, Y. Wu, *Nanoscale* **2012**, *4*, 2251.
[17] P.-C. Chen, T.-Y. Yeh, C.-M. Ou, C.-C. Shih, H.-T. Chang, *Nanoscale* **2013**, *5*, 4691.
[18] J. M. Obliosca, C. Liu, H.-C. Yeh, *Nanoscale* **2013**, *5*, 8443.
[19] A. Coskun, E. U. Akkaya, *J. Am. Chem. Soc.* **2005**, *127*, 10464.
[20] Y. Hong, J. W. Y. Lam, B. Z. Tang, *Chem. Soc. Rev.* **2011**, *40*, 5361.
[21] Y. Liu, Y. Tang, N. N. Barashkov, I. S. Irgibaeva, J. W. Y. Lam, R. Hu, D. Birimzhanova, Y. Yu, B. Z. Tang, *J. Am. Chem. Soc.* **2010**, *132*, 13951.
[22] V. K. Bhardwaj, H. Sharma, N. Kaur, N. Singh, *New J. Chem.* **2013**, *37*, 4192.
[23] A. Singh, S. Kaur, N. Singh, N. Kaur, *Org. Biomol. Chem.* **2014**, *12*, 2302.
[24] A. Singh, V. K. Bhardwaj, G. Kaur, K. Kaur, N. Singh, M. S. Bakshi, *RSC Adv.* **2014**, *4*, 21079.
[25] A. Singh, S. Kaur, A. Kaur, T. Aree, N. Kaur, N. Singh, M. S. Bakshi, *ACS Sustainable Chem. Eng.* **2014**, *2*, 982.
[26] A. Singh, T. Raj, T. Aree, N. Singh, *Eur. J. Inorg. Chem.* **2013**, *52*, 13830.
[27] F. Qu, J. a. Liu, H. Yan, L. Peng, H. Li, *Tetrahedron Lett.* **2008**, *49*, 7438.
[28] V. K. Bhardwaj, A. P. S. Pannu, N. Singh, M. S. Hundal, G. Hundal, *Tetrahedron* **2008**, *64*, 5384.
[29] A. W. Van der Made, R. H. Van der Made, *J. Org. Chem.* **1993**, *58*, 1262.
[30] H. Sharma, N. Kaur, N. Singh, *Inorg. Chim. Acta* **2012**, *391*, 83.
[31] E. R. Triboni, P. B. Filho, R. G. de Souza Berlinck, M. J. Politi, *Synth. Commun.* **2004**, *34*, 1989.
[32] S. Yagai, Y. Goto, X. Lin, T. Karatsu, A. Kitamura, D. Kuzuhara, H. Yamada, Y. Kikkawa, A. Saeki, S. Seki, *Angew. Chem. Int. Ed.* **2012**, *51*, 6643.

[33] Q. Zeng, Z. Li, Y. Dong, C. A. Di, A. Qin, Y. Hong, L. Ji, Z. Zhu, C. K. W. Jim, G. Yu, Q. Li, Z. Li, Y. Liu, J. Qin, B. Z. Tang, *Chem. Commun.* **2007**, 70.
[34] T. H. Kim, S. H. Kim, L. V. Tan, Y. J. Seo, S. Y. Park, H. Kim, J. S. Kim, *Talanta* **2007**, *71*, 1294.
[35] S. S. Lehrer, G. D. Fasman, *Biochem. Biophys. Res. Commun.* **1966**, *23*, 133.
[36] D. M. Chipman, V. Grisaro, N. Sharon, *J. Biol. Chem.* **1967**, *242*, 4388.
[37] A. D. Becke, *J. Chem. Phys.* **1993**, *98*, 5648.
[38] C. Lee, W. Yang, R. G. Parr, *Phys. Rev. B* **1988**, *37*, 785.
[39] P. J. Hay, W. R. Wadt, *J. Chem. Phys.* **1985**, *82*, 299.
[40] W. R. Wadt, P. J. Hay, *J. Chem. Phys.* **1985**, *82*, 284.
[41] P. J. Hay, W. R. Wadt, *J. Chem. Phys.* **1985**, *82*, 270.

Received: May 28, 2014
Published Online: September 29, 2014

